

The Kelvin-Helmholtz instability at the boundary of relativistic magnetized jets

Anthony Chow,^{1,*} Jordy Davelaar,^{1,2,†} and Lorenzo Sironi^{1,‡}

¹*Department of Astronomy and Columbia Astrophysics Laboratory,
Columbia University, New York, NY 10027, USA*

²*Center for Computational Astrophysics, Flatiron Institute, 162 Fifth Avenue, New York, NY 10010, USA*
(Dated: September 29, 2022)

We study the linear stability of a planar interface separating two fluids in relative motion, focusing on conditions appropriate for the boundaries of relativistic jets. The jet is magnetically dominated, whereas the ambient wind is gas-pressure dominated. We derive the most general form of the dispersion relation and provide an analytical approximation of its solution for an ambient sound speed much smaller than the jet Alfvén speed v_A , as appropriate for realistic systems. The stability properties are chiefly determined by the angle ψ between the wavevector and the jet magnetic field. For $\psi = \pi/2$, magnetic tension plays no role, and our solution resembles the one of a gas-pressure dominated jet. Here, only sub-Alfvénic jets are unstable ($0 < M_e \equiv (v/v_A) \cos \theta < 1$, where v is the shear velocity and θ the angle between the velocity and the wavevector). For $\psi = 0$, the free energy in the velocity shear needs to overcome the magnetic tension, and only super-Alfvénic jets are unstable ($1 < M_e < \sqrt{(1 + \Gamma_w^2)/[1 + (v_A/c)^2 \Gamma_w^2]}$, with Γ_w the wind adiabatic index). Our results have important implications for the propagation and emission of relativistic magnetized jets.

The Kelvin-Helmholtz instability (KHI) [1, 2]— at the interface of two fluids in relative motion — is one of the most ubiquitous and well-studied instabilities in the Universe. Since the pioneering works of Chandrasekhar [3], the linear theory of the KHI has been investigated under a variety of conditions [4–18], depending on whether the relative motion is non-relativistic or ultra-relativistic, whether the two fluids have comparable or different properties (respectively, “symmetric” or “asymmetric” configuration), whether the flow is incompressible or compressible, and whether or not the fluids are magnetized.

The boundaries of relativistic astrophysical jets may be prone to the KHI, given the relative (generally, ultra-relativistic) shear velocity between the jet and the ambient medium (hereafter, the “wind”). In jet boundaries with flow-aligned magnetic fields, KH vortices can wrap up the field lines onto themselves, leading to particle acceleration via reconnection [19]. Particles pre-energized by reconnection [e.g., 20–22] can then experience shear-driven acceleration [23, 24] — i.e., particles scatter in between regions that move toward each other because of the velocity shear, akin to the Fermi process in converging flows [25]. The KHI may then constitute a fundamental building block for our understanding of the origin of radio-emitting electrons in limb-brightened relativistic jets (e.g., in Cygnus A [26] and M87 [27]), and for the prospects of shear-driven acceleration at jet boundaries in generating Ultra High Energy Cosmic Rays.

A study of the KHI in this context needs to account for the unique properties of the boundaries of relativistic jets. First, the relative motion between the jet and the wind can be ultra-relativistic; second, while the wind is likely gas-pressure dominated, relativistic jets are believed to be magnetically dominated [28] (hence, an asymmetric configuration). The linear stability properties of the KHI in this regime (of relativistic, asymmet-

ric, magnetized flows) are still unexplored. In this *Letter*, we derive the most general form of the dispersion relation for the KHI at the interface between a magnetized relativistic jet and a gas-pressure-dominated wind. We also provide an analytical approximation of its solution for wind sound speeds much smaller than the jet Alfvén speed, as appropriate for realistic astrophysical systems.

Setup—We consider a planar vortex-sheet interface in the x - z plane at $y = 0$. The jet ($y > 0$) is cold and magnetized, with field $\mathbf{B}_{0j} = (B_{0x}, 0, B_{0z})$ lying in the x - z plane, and Alfvén speed v_A . The ambient wind ($y < 0$) is gas-pressure supported (with sound speed c_{sw}) and has a vanishing magnetic field. We use the subscript “ j ” for the jet and “ w ” for the wind. We solve the system in the jet rest frame, where the wind moves with velocity $\mathbf{v} = v \hat{x}$. We adopt Gaussian units such that $c = 4\pi = 1$ and define all velocities in unit of c .

We describe the flow with the equations of relativistic magnetohydrodynamics (RMHD) [e.g., 29]:

$$\frac{\partial(\rho\gamma)}{\partial t} + \nabla \cdot (\rho\gamma\mathbf{v}) = 0 \quad (1a)$$

$$\frac{\partial}{\partial t}(w\gamma^2\mathbf{v}) + \nabla \cdot (w\gamma^2\mathbf{v}\mathbf{v}) + \nabla p = \rho_e\mathbf{E} + \mathbf{J} \times \mathbf{B} \quad (1b)$$

$$\frac{\partial\mathbf{B}}{\partial t} + \nabla \times \mathbf{E} = 0 \quad (1c)$$

$$\frac{\partial\mathbf{E}}{\partial t} - \nabla \times \mathbf{B} = -\mathbf{J} \quad (1d)$$

$$\frac{\partial}{\partial t}(w\gamma^2 - p) + \nabla \cdot (w\gamma^2\mathbf{v}) = \mathbf{J} \cdot \mathbf{E} \quad (1e)$$

supplemented with the divergence constraints

$$\nabla \cdot \mathbf{E} = \rho_e, \quad \nabla \cdot \mathbf{B} = 0 \quad (2)$$

Here, ρ , ρ_e , \mathbf{J} , \mathbf{v} , γ , \mathbf{B} , \mathbf{E} , w and p are the rest-mass density, charge density, current density, fluid velocity, Lorentz factor ($\gamma = 1/\sqrt{1 - v^2}$), magnetic field, electric

field, gas enthalpy density and pressure, respectively. For an ideal gas with adiabatic index Γ , the enthalpy can be written as $w = \rho + \Gamma p / (\Gamma - 1)$.

We assume a cold and magnetically-dominated jet, with Alfvén speed $v_A^2 = v_{A,\text{in}}^2 + v_{A,\text{out}}^2$, where

$$v_{A,\text{in}} = \sqrt{\frac{B_{0x}^2}{w_{0j} + B_{0x}^2 + B_{0z}^2}}, \quad v_{A,\text{out}} = \sqrt{\frac{B_{0z}^2}{w_{0j} + B_{0x}^2 + B_{0z}^2}} \quad (3)$$

and the jet enthalpy density is $w_{0j} \approx \rho_{0j}$ for a cold jet. The wind has negligible magnetic field and is gas-pressure supported, with sound speed [29]

$$c_{sw} = \sqrt{\frac{w_{0w} - \rho_{0w}(\partial w_{0w}/\partial \rho_{0w})}{(\partial w_{0w}/\partial p_{0w}) - 1}} \frac{1}{w_{0w}} = \sqrt{\Gamma_w \frac{p_{0w}}{w_{0w}}} \quad (4)$$

where w_{0w} is the wind enthalpy density. From pressure balance across the interface,

$$\frac{1}{2}(B_{0x}^2 + B_{0z}^2) = \frac{c_{sw}^2 w_{0w}}{\Gamma_w} \Rightarrow \frac{w_{0w}}{w_{0j}} = \frac{1}{2} \frac{v_A^2 \Gamma_w}{(1 - v_A^2) c_{sw}^2}, \quad (5)$$

where Γ_w is the wind adiabatic index.

Dispersion relation—The dispersion relation of surface waves at the interface can be found from the dispersion relations of body waves in both the jet and the ambient wind, together with the displacement matching at the interface. The dispersion relations of body waves in each of the two fluids can be found by linearizing Eqs. (1), such that the perturbed variables take the form $\varphi \approx \varphi_0 + \varphi_1$, where φ_0 and φ_1 are the background and the first-order perturbed variables respectively. The perturbed electric field in the jet is $\mathbf{E}_1 = -\mathbf{v}_1 \times \mathbf{B}_{0j}$ in the ideal MHD limit, where \mathbf{v}_1 is the perturbed velocity in the jet frame.

In the jet, we consider perturbed variables φ_1 of the form $\varphi_1 \propto e^{i(\mathbf{q}\cdot\mathbf{x} - \omega t)}$ where $\mathbf{q} = (k, l_j, m)$ is the complex wavevector and ω is the complex angular frequency, both defined in the jet rest frame. Note that $\text{Im}(\omega) > 0$ implies that the amplitude of the wave grows exponentially, i.e., an instability. We define the angle θ between the projection of the wavevector onto the x - z plane and the direction \hat{x} of the shear flow velocity such that

$$\cos \theta = \frac{k}{\sqrt{k^2 + m^2}}. \quad (6)$$

Similarly, we define the angle ψ between the wavevector projection onto the x - z plane and the jet magnetic field such that

$$\cos \psi = \frac{kv_{A,\text{in}} + mv_{A,\text{out}}}{v_A \sqrt{k^2 + m^2}}. \quad (7)$$

For a magnetized cold jet, the dispersion relation of its body waves describes magnetosonic waves in the cold

plasma limit:

$$\omega[\omega^2 - (kv_{A,\text{in}} + mv_{A,\text{out}})^2] \\ [\omega^2 - (k^2 + l_j^2 + m^2)v_A^2] = 0. \quad (8)$$

In the wind, we consider perturbed variables φ_1 of the form $\varphi_1 \propto e^{i(\tilde{\mathbf{q}}\cdot\mathbf{x} - \tilde{\omega}t)}$ where $\tilde{\mathbf{q}} = (\tilde{k}, l_w, m)$ is the complex wavevector and $\tilde{\omega}$ is the complex angular frequency, both defined in the wind rest frame. For an unmagnetized wind, the dispersion relation of its body waves reduces to the one of sound waves, $\tilde{\omega}^2 - (\tilde{k}^2 + l_w^2 + m^2)c_{sw}^2 = 0$. By Lorentz transformations of $\tilde{\omega} = \gamma(\omega - kv)$ and $\tilde{k} = \gamma(k - v\omega)$, we obtain

$$\gamma^2(\omega - kv)^2 = c_{sw}^2[l_w^2 + m^2 + \gamma^2(k - v\omega)^2]. \quad (9)$$

Since l_j and l_w are Lorentz invariant, by solving Eq. (8) and Eq. (9) for l_j and l_w respectively, we can construct a Lorentz invariant ratio:

$$\frac{l_w^2}{l_j^2} = \frac{v_A^2[\gamma^2(\omega - kv)^2 - c_{sw}^2(m^2 + \gamma^2(k - v\omega)^2)]}{c_{sw}^2[\omega^2 - (k^2 + m^2)v_A^2]} \quad (10)$$

An independent way of obtaining l_w/l_j is to simultaneously solve the linearized RMHD equations, Eqs. (1), together with the first order pressure balance equation

$$B_{0x}B_{1x} + B_{0z}B_{1z} = p_{1w} \quad (11)$$

and the displacement matching condition at the interface

$$\frac{v_{1y,j}}{\omega} = \frac{v_{1y,w}}{\gamma(\omega - kv)}, \quad (12)$$

yielding

$$\frac{l_w}{l_j} = \frac{\gamma^2(1 - v_A^2)(\omega - kv)^2}{\omega^2 - (kv_{A,\text{in}} + mv_{A,\text{out}})^2} \frac{w_{0w}}{w_{0j}}. \quad (13)$$

Using Eq. (5), we can eliminate w_{0w}/w_{0j} from Eq. (13) and finally, the dispersion relation for the surface wave at the interface can be obtained by equating Eq. (10) and the square of Eq. (13):

$$\frac{\gamma^2(\omega - kv)^2 - c_{sw}^2(m^2 + \gamma^2(k - v\omega)^2)}{\omega^2 - (k^2 + m^2)v_A^2} \\ = \frac{1}{4} \frac{v_A^2 \gamma^4 (\omega - kv)^4 \Gamma_w^2}{[\omega^2 - (kv_{A,\text{in}} + mv_{A,\text{out}})^2]^2 c_{sw}^2}. \quad (14)$$

By introducing the following notations,

$$\phi = \frac{\omega}{v_A \sqrt{k^2 + m^2}}, \quad M = \frac{v}{v_A}, \quad \eta = v_A, \quad \epsilon = \frac{c_{sw}}{v_A}, \quad (15)$$

Eq. (14) can be rewritten as

$$4\epsilon^2(1 - M^2\eta^2)(\cos^2 \psi - \phi^2)^2 \\ [\epsilon^2(1 - 2M\eta^2\phi \cos \theta + M^2\eta^2(\cos^2 \theta - 1 + \eta^2\phi^2)) \\ - (M \cos \theta - \phi)^2] = (M \cos \theta - \phi)^4(1 - \phi^2)\Gamma_w^2 \quad (16)$$

The dispersion relation in Eq. (16) is the main result of this study. It holds for arbitrary values of c_{sw} , v_A , v , $\cos\theta$ and $\cos\psi$, subject only to the assumptions of a cold jet and an unmagnetized wind.

Since Eq. (16) is a sextic equation in ϕ , it has a total of six (generally, complex) roots. However, not all of them may be acceptable. First, not all of the solutions will satisfy Eq. (13), since we have introduced spurious roots when squaring it. Also, by the Sommerfeld radiation condition [30], only outgoing waves should be retained. This requires $\text{Im}(l_w) < 0$ and $\text{Im}(l_j) > 0$. The expressions for l_w and l_j can be obtained from the derivation of Eq. (13), so the Sommerfeld condition can be expressed as

$$\text{Im}(l_w) = \text{Im}\left(\frac{(\phi - M \cos\theta)^2}{\phi}\right) < 0 \quad (17a)$$

$$\text{Im}(l_j) = \text{Im}\left(\frac{\phi^2 - \cos^2\psi}{\phi}\right) > 0 \quad (17b)$$

Analytical approximation—Since in general a sextic equation has no algebraic roots [31], only approximate solutions of ϕ in Eq. (16) can be obtained. We first note that the parameters in Eq. (15) are chosen such that for a realistic wind with $c_{sw} \ll v_A$, we have $\epsilon \ll 1$, whereas the other parameters do not depend on c_{sw} . We then expand ϕ as a power series of ϵ of the form $\phi \approx c_0 + c_1\epsilon + c_2\epsilon^2$, where c_0, c_1 and c_2 are constant with respect to ϵ and terms higher than ϵ^2 are ignored. Substituting this into Eq. (16) and comparing coefficients of various powers of ϵ on both sides, we can find an approximate solution for all six roots of Eq. (16). If we denote

$$M_e \equiv M \cos\theta, \quad (18)$$

$\mu \equiv \cos^2\psi - M_e^2$, and recognize that $\gamma^{-2} = 1 - M^2\eta^2$, then the approximate roots can be written as:

$$\phi_{1,2} = \mp 1 \mp \frac{2(1 - \cos^2\psi)^2}{\gamma^2(1 \pm M_e)^2\Gamma_w^2}\epsilon^2, \quad (19a)$$

$$\phi_{3,4} = M_e \mp \Lambda_- \epsilon + \Sigma_- \epsilon^2, \quad (19b)$$

$$\phi_{5,6} = M_e \mp \Lambda_+ \epsilon - \Sigma_+ \epsilon^2 \quad (19c)$$

where

$$\Lambda_{\pm} = \sqrt{-\frac{\mu^2 \pm \lambda}{\gamma^2(1 - M_e^2)\Gamma_w^2}}, \quad (20)$$

$$\lambda = \sqrt{\mu^4 + \mu^2(1 - M_e^2)(1 - M_e^2\eta^2)\Gamma_w^2}. \quad (21)$$

The solutions $\phi_{1,2}$ in Eq. (19) correspond to stable modes, so only $\phi_{3,4}$ and $\phi_{5,6}$ are relevant for our study. For them, we find that the first order term $\Lambda_{\pm}\epsilon$ generally provides a good approximation of the numerical solution for ϕ . However, the second order term (which we write explicitly in the Suppl. Mat.) is required for identifying the physical solutions that satisfy Eq. (13) and the Sommerfeld condition. In Fig. 1 and Fig. 2, we compare the numerical solution (left column) of Eq. (16)

with our analytical approximation (right column). We fix $c_{sw} = 0.005$ and consider $v_A = 0.2$ and 0.8 , so the assumption $c_{sw}/v_A \ll 1$ of our analytical approximation is well satisfied. The analytical solution for $\text{Im}(\phi)$ displayed in the figures only employs the first order terms (as discussed above, we also use the second order terms to check the Sommerfeld constraint), yet it provides an excellent approximation of the numerical results, apart from $M_e = 1$. For $M_e = 1$, the first-order term Λ_{\pm} of our analytical approximation diverges. We discuss below this special case.

Our analytical approximation allows to determine the range of M_e where the system is unstable. If λ in Eq. (21) is imaginary, then also Λ_{\pm} has nonzero imaginary part. We then find the values of M_e that satisfy $\lambda^2 = 0$ and obtain the following unstable bounds: for $M_e < 1$,

$$\cos\psi < M_e < \min\left(\frac{\cos\theta}{\eta}, 1\right), \quad (22)$$

whereas for $M_e > 1$

$$\sqrt{\frac{\nu_1 - \nu_2}{2 + 2\eta^2\Gamma_w^2}} < M_e < \min\left(\frac{\cos\theta}{\eta}, \sqrt{\frac{\nu_1 + \nu_2}{2 + 2\eta^2\Gamma_w^2}}\right), \quad (23)$$

where

$$\nu_1 = 2\cos^2\psi + (1 + \eta^2)\Gamma_w^2 \quad (24)$$

$$\nu_2 = \sqrt{(1 - \eta^2)^2\Gamma_w^4 - 4(1 - \cos^2\psi)(1 - \eta^2\cos^2\psi)\Gamma_w^2}$$

Note that the condition $M_e < \cos\theta/\eta$ is equivalent to the obvious requirement $v < 1$. Eq. (22) and Eq. (23) fully characterize the instability boundaries in Fig. 1 and Fig. 2. In particular, the vertical white dotted lines in the figures illustrate the upper bound in Eq. (23) for the special case $\cos\psi = 1$, which yields

$$1 < M_e < \min\left(\frac{\cos\theta}{\eta}, \sqrt{\frac{1 + \Gamma_w^2}{1 + \eta^2\Gamma_w^2}}\right) \quad \text{for } \cos\psi = 1. \quad (25)$$

It follows that the unstable range at $M_e > 1$ shrinks for $\eta = v_A \rightarrow 1$, but never disappears.

The special case $M_e = 1$ —In the case $M_e = 1$, our analytical approximation diverges. The singular case $M_e = 1$ can be solved by expanding ϕ with a Puiseux series [32, 33]. We obtain the following first order approximate solutions of ϕ at $M_e = 1$:

$$\phi_1 = -1, \quad (26a)$$

$$\phi_{2,3} = 1 \pm \frac{\sqrt{\cos^2\theta - \eta^2}\sqrt{\eta^2 - 1}}{\cos\theta}\epsilon, \quad (26b)$$

$$\phi_{4,5} = 1 \pm (\pm 2\xi)^{1/3}\epsilon^{2/3}, \quad (26c)$$

$$\phi_6 = 1 + (-1)^{2/3}(2\xi)^{1/3}\epsilon^{2/3} \quad (26d)$$

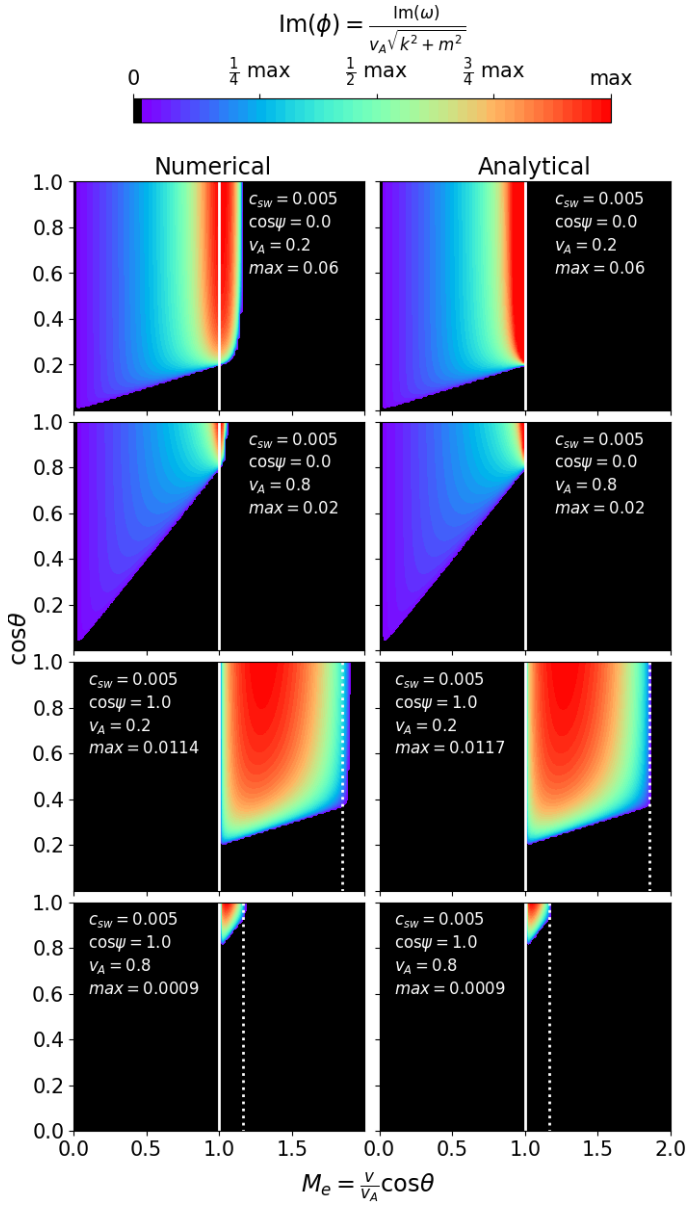


FIG. 1. Dependence of the instability growth rate $\text{Im}(\phi)$ on θ and M_e , for two choices of v_A and two choices of $\cos\psi$, as indicated in the plots. The left and right columns represent the numerical and analytical solutions, respectively. For $\cos\psi = 0$, the maximum growth rate of the analytical solution is capped at its numerical counterpart to avoid the divergence at $M_e = 1$. In all the panels, $\text{Im}(\phi)$ is then normalized to its maximum value, which is quoted in the panels themselves. The vertical dotted lines show the analytical upper bound on M_e when $\cos\psi = 1$, see Eq. (25).

where

$$\xi = \frac{(\cos^2\psi - 1)^2(\cos^2\theta - \eta^2)}{\Gamma_w^2 \cos^2\theta}. \quad (27)$$

In Suppl. Mat. we demonstrate that this analytical approximation for the special case $M_e = 1$ is in good agreement with the numerical solution.

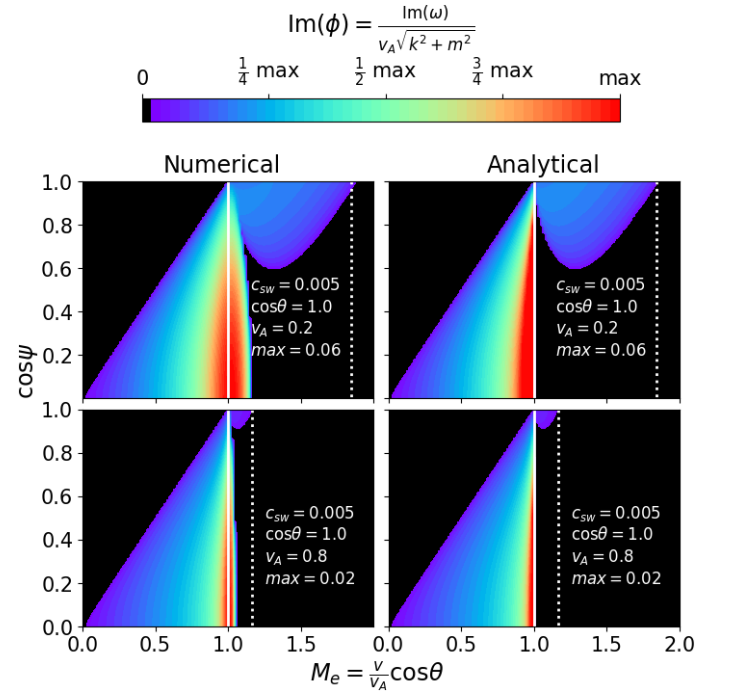


FIG. 2. Dependence of the instability growth rate $\text{Im}(\phi)$ on ψ and M_e , for two choices of v_A as indicated in the plots. We fix $\cos\theta = 1$. See the caption of Fig. 1 for further details.

Comparison to the hydrodynamic case—When the unstable mode propagates perpendicularly to the magnetic field ($\cos\psi = 0$), we expect magnetic tension to have no effect, and the solution should resemble the hydrodynamic asymmetric case discussed by [5]. We demonstrate this by choosing a different parameterization in Eq. (16), similar to the one of Eq. (2) in [5], i.e.

$$\begin{aligned} \epsilon' &= \frac{1}{\epsilon} = \frac{v_A}{c_{sw}}, & \phi' &= \frac{\phi}{\epsilon} = \frac{\omega}{c_{sw}\sqrt{k^2 + m^2}}, \\ \delta' &= \frac{w_{0w}}{w_{0j}^*} \frac{c_{sw}^2}{v_A^2}, & \eta' &= \eta\epsilon = c_{sw}, \\ M' &= \frac{M \cos\theta}{\epsilon} = \frac{v}{c_{sw}} \frac{k}{\sqrt{k^2 + m^2}}, \end{aligned} \quad (28)$$

where w_{0j}^* is the total enthalpy of the jet, namely the sum of the gas enthalpy w_{0j} and the magnetic enthalpy:

$$w_{0j}^* = B_{0x}^2 + B_{0z}^2 + w_{0j} = \frac{w_{0j}}{1 - v_A^2}. \quad (29)$$

Then the dispersion relation Eq. (16) can be equivalently written as

$$\begin{aligned} &(\phi'^2 - \cos^2\psi)^2[\gamma^2(1 - \eta'^2)(\phi' - M')^2 + \eta'^2\phi'^2 - 1] \\ &= \gamma^4\delta'^2(\phi' - M')^4(\phi'^2 - \epsilon'^2)\epsilon'^2, \end{aligned} \quad (30)$$

which, by setting $\cos\psi = 0$, is exactly the same as Eq. (1) in [5], where both the jet and the wind were assumed to be unmagnetized. We conclude that, even though our jet

is magnetized, in the case $\cos \psi = 0$ the instability behaves similarly to the case of a hydrodynamic jet. Here, the magnetic field provides pressure, but not tension.

Conclusions— We have studied the linear stability properties of the KHI for relativistic, asymmetric, magnetized flows, with focus on conditions appropriate for the interface between a magnetized relativistic jet and a gas-pressure-dominated wind. We derive the most general form of the dispersion relation and provide an analytical approximation of its solution for $c_{sw}/v_A \ll 1$. The stability properties are chiefly determined by the angle ψ between the jet magnetic field and the wavevector projection onto the jet/wind interface. For $\psi = \pi/2$, magnetic tension plays no role, and our solution resembles the one of a gas-pressure dominated jet. Here, only sub-Alfvénic jets are unstable ($0 < M_e \equiv (v/v_A) \cos \theta < 1$, as long as $v < 1$). For $\psi = 0$, the velocity shear needs to overcome the magnetic tension, and only super-Alfvénic jets are unstable ($1 < M_e < \sqrt{(1 + \Gamma_w^2)/(1 + v_A^2 \Gamma_w^2)}$).

Our analytical results are valuable for both theoretical and observational studies. They can be easily incorporated into global MHD simulations of jet launching and propagation, to identify KH-unstable surfaces [19, 34, 35]. On the observational side, claims have been made that the KHI is observed along Active Galactic Nuclei (AGN) jets, based on the geometry of the outflow [36, 37]. Our formulae can place this claim on solid grounds, if estimates of the field strength and orientation and of the flow velocities are available. Besides AGNs, our results have implications for other jetted sources such as, but not limited to, gamma-ray bursts, tidal disruption events, X-ray binaries, and pulsar wind nebulae.

We conclude with a few caveats. First, the plane-parallel approach we employed is applicable only if the jet/wind interface is much narrower than the jet radius. Secondly, our local description implicitly assumes that the flow properties do not change as the KHI grows, i.e., that the growth time is faster than the jet propagation time. Third, we have assumed the jet plasma to be cold, and the surrounding medium to be unmagnetized. These assumptions will be relaxed in a future work.

We are grateful to M. Rowan and R. Narayan for collaborations on this topic. L.S. acknowledges support from the Cottrell Scholars Award, and Doe DESC0023015. L.S. and J.D. acknowledge support from NSF AST-2108201, NSF PHY-1903412 and NSF PHY-2206609. J.D. is supported by a Joint Columbia University/Flatiron Research Fellowship, research at the Flatiron Institute is supported by the Simons Foundation.

* kc3058@columbia.edu

† jrd2210@columbia.edu

- ‡ lsironi@astro.columbia.edu
- [1] H. Von Helmholtz and K. Monats, Preuss. Akad. Wiss. Berlin **23**, 215 (1868).
 - [2] Lord Kelvin, Philos. Mag. **42**, 362 (1871).
 - [3] S. Chandrasekhar, *Hydrodynamic and Hydromagnetic stability* (Clarendon Press, 1961).
 - [4] B. D. Turland and P. A. Scheuer, Instabilities of kelvin-helmholtz type for relativistic streaming, *Monthly Notices of the Royal Astronomical Society* **176**, 421–441 (1976).
 - [5] R. D. Blandford and J. E. Pringle, Kelvin-helmholtz instability of relativistic beams, *Monthly Notices of the Royal Astronomical Society* **176**, 443–454 (1976).
 - [6] A. Ferrari, E. Trussoni, and L. Zaninetti, Magnetohydrodynamic kelvin-helmholtz instabilities in astrophysics – i. relativistic flows–plane boundary layer in vortex sheet approximation, *Monthly Notices of the Royal Astronomical Society* **193**, 469–486 (1980).
 - [7] Z.-Y. Pu and M. G. Kivelson, Kelvin-helmholtz instability at the magnetopause: Solution for compressible plasmas, *Journal of Geophysical Research* **88**, 841 (1983).
 - [8] M. G. Kivelson and P. Zu-Yin, The kelvin-helmholtz instability on the magnetopause, *Planetary and Space Science* **32**, 1335–1341 (1984).
 - [9] G. Bodo, A. Mignone, and R. Rosner, Kelvin-Helmholtz instability for relativistic fluids, *Phys. Rev. E* **70**, 036304 (2004).
 - [10] Z. Osmanov, A. Mignone, S. Massaglia, G. Bodo, and A. Ferrari, On the linear theory of kelvin-helmholtz instabilities of relativistic magnetohydrodynamic planar flows, *Astronomy and Astrophysics* **490**, 493–500 (2008).
 - [11] W. Blumen, P. G. Drazin, and D. F. Billings, Shear layer instability of an inviscid compressible fluid. Part 2, *Journal of Fluid Mechanics* **71**, 305 (1975).
 - [12] A. Ferrari, E. Trussoni, and L. Zaninetti, Relativistic Kelvin-Helmholtz instabilities in extragalactic radio sources., *A&A* **64**, 43 (1978).
 - [13] P. K. Sharma and R. K. Chhajlani, Kelvin-Helmholtz instability of magnetized plasma with polytropic pressure laws, *Physics of Plasmas* **5**, 625 (1998).
 - [14] S. S. Komissarov, *MNRAS* **303**, 343 (1999).
 - [15] R. P. Prajapati and R. K. Chhajlani, Effect of pressure anisotropy and flow velocity on kelvin-helmholtz instability of anisotropic magnetized plasma using generalized polytropic laws, *Physics of Plasmas* **17**, 112108 (2010), <https://doi.org/10.1063/1.3512936>.
 - [16] E. Sobacchi and Y. E. Lyubarsky, External confinement and surface modes in magnetized force-free jets, *MNRAS* **473**, 2813 (2018).
 - [17] T. Berlok and C. Pfrommer, On the Kelvin-Helmholtz instability with smooth initial conditions - linear theory and simulations, *MNRAS* **485**, 908 (2019), [arXiv:1902.01403 \[astro-ph.GA\]](https://arxiv.org/abs/1902.01403).
 - [18] M. E. Rowan, *Dissipation of magnetic energy in collisionless accretion flows*, Ph.D. thesis, Harvard University, Massachusetts (2019).
 - [19] L. Sironi, M. E. Rowan, and R. Narayan, Reconnection-driven Particle Acceleration in Relativistic Shear Flows, *ApJ* **907**, L44 (2021), [arXiv:2009.11877 \[astro-ph.HE\]](https://arxiv.org/abs/2009.11877).
 - [20] L. Sironi and A. Spitkovsky, Relativistic Reconnection: An Efficient Source of Non-thermal Particles, *ApJ* **783**, L21 (2014), [arXiv:1401.5471 \[astro-ph.HE\]](https://arxiv.org/abs/1401.5471).
 - [21] H. Zhang, L. Sironi, and D. Giannios, Fast Particle Acceleration in Three-dimensional Relativistic Reconnection,

- Astrophys. J.* **922**, 261 (2021), arXiv:2105.00009 [astro-ph.HE].
- [22] L. Sironi, Nonideal Fields Solve the Injection Problem in Relativistic Reconnection, *Phys. Rev. Lett.* **128**, 145102 (2022), arXiv:2203.04342 [astro-ph.HE].
- [23] F. M. Rieger, An Introduction to Particle Acceleration in Shearing Flows, *Galaxies* **7**, 78 (2019), arXiv:1909.07237 [astro-ph.HE].
- [24] J.-S. Wang, B. Reville, R.-Y. Liu, F. M. Rieger, and F. A. Aharonian, Particle acceleration in shearing flows: the case for large-scale jets, *MNRAS* **505**, 1334 (2021), arXiv:2105.08600 [astro-ph.HE].
- [25] E. Fermi, On the Origin of the Cosmic Radiation, *Physical Review* **75**, 1169 (1949).
- [26] B. Boccardi, T. P. Krichbaum, U. Bach, F. Mertens, E. Ros, W. Alef, and J. A. Zensus, The stratified two-sided jet of Cygnus A. Acceleration and collimation, *A&A* **585**, A33 (2016), arXiv:1509.06250 [astro-ph.HE].
- [27] R. C. Walker, P. E. Hardee, F. B. Davies, C. Ly, and W. Junor, The Structure and Dynamics of the Subparsec Jet in M87 Based on 50 VLBA Observations over 17 Years at 43 GHz, *Astrophys. J.* **855**, 128 (2018), arXiv:1802.06166 [astro-ph.HE].
- [28] R. D. Blandford and R. L. Znajek, Electromagnetic extraction of energy from Kerr black holes, *MNRAS* **179**, 433 (1977).
- [29] A. Mignone, G. Mattia, and G. Bodo, Linear wave propagation for resistive relativistic magnetohydrodynamics, *Physics of Plasmas* **25**, 092114 (2018).
- [30] A. Sommerfeld, Die Greensche Funktion der Schwingungsgleichung, *Jhrber. German. Math.-Verein* **12**, 309 (1912).
- [31] N. H. Abel, Beweis der unmöglichkeit, algebraische gleichungen von höheren graden als dem vierten allgemein aufzulösen., *Journal für die reine und angewandte Mathematik (Crelles Journal)* **1826**, 65–84 (1826).
- [32] C. T. C. Wall, Puiseux' theorem, in *Singular Points of Plane Curves*, London Mathematical Society Student Texts (Cambridge University Press, 2004) p. 15–38.
- [33] W. Research, AsymptoticSolve, <https://reference.wolfram.com/language/ref/AsymptoticSolve.html> (2020).
- [34] K. Chatterjee, S. Markoff, A. Tchekhovskoy, M. Liska, Z. Younsi, and D. Yoon, Black hole AGN jets from the event horizon to parsec scales, in *American Astronomical Society Meeting Abstracts #235*, American Astronomical Society Meeting Abstracts, Vol. 235 (2020) p. 411.05.
- [35] G. N. Wong, Y. Du, B. S. Prather, and C. F. Gammie, The Jet-disk Boundary Layer in Black Hole Accretion, *Astrophys. J.* **914**, 55 (2021), arXiv:2104.07035 [astro-ph.HE].
- [36] A. P. Lobanov and J. A. Zensus, A Cosmic Double Helix in the Archetypical Quasar 3C273, *Science* **294**, 128 (2001).
- [37] S. Issaoun, M. Wielgus, S. Jorstad, T. P. Krichbaum, L. Blackburn, M. Janssen, C.-k. Chan, D. W. Pesce, J. L. Gómez, K. Akiyama, M. Mościbrodzka, I. Martí-Vidal, A. Chael, R. Lico, J. Liu, V. Ramakrishnan, M. Lisakov, A. Fuentes, G.-Y. Zhao, K. Moriyama, A. E. Broderick, P. Tiede, N. R. MacDonald, Y. Mizuno, E. Traianou, L. Loinard, J. Davelaar, M. Gurwell, R.-S. Lu, and the EHTC, Resolving the Inner Parsec of the Blazar J1924-2914 with the Event Horizon Telescope, *Astrophys. J.*

934, 145 (2022), arXiv:2208.01662 [astro-ph.HE].

SUPPLEMENTARY MATERIAL

Analytical approximation for $M_e = 1$

For the singular case $M_e = 1$, our analytical solutions take the form of the first order Puiseux series. Here we compare the analytical and numerical solutions. In Fig. 3 and Fig. 4, we plot the instability growth rate for $M_e = 1$, comparing analytical and numerical solutions. We choose the same parameters as in the figures of the main paper, namely $c_{sw} = 0.005$, and $v_A = 0.2$ or 0.8 . We fix $\cos\psi = 0$ for Fig. 3 and $\cos\theta = 1$ for Fig. 4. We use solid and dashed lines to represent numerical and analytical solutions, respectively. The figures show that our analytical solutions in Puiseux series provide a good approximation to the numerical ones across the entire range of $\cos\theta$ (for Fig. 3) and $\cos\psi$ (for Fig. 4).

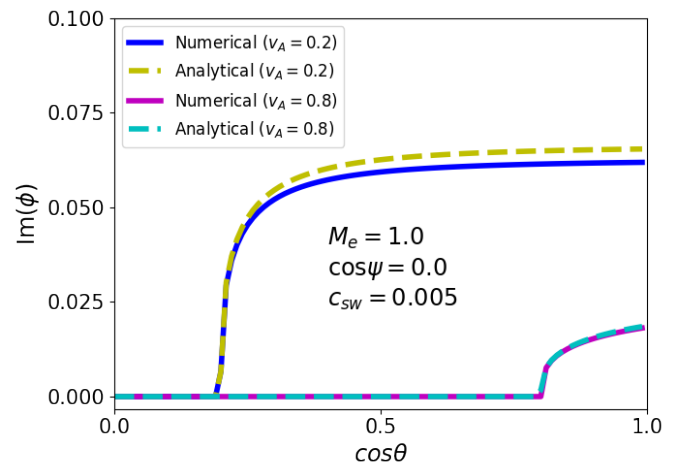


FIG. 3. Dependence of the instability growth rate $\text{Im}(\phi)$ on $\cos\theta$ for two choices of v_A and a fixed value of $\cos\psi = 0$ in the singular case $M_e = 1$. Solid lines represent the numerical solutions while dashed lines represent the analytical solutions obtained by Puiseux series expansion in the main text.

The second order terms

In the main body of the paper, we have looked for an analytical approximation of the form $\phi \approx c_0 + c_1\epsilon + c_2\epsilon^2$, where c_0, c_1 and c_2 are constant with respect to ϵ and terms higher than ϵ^2 are ignored. For the unstable solutions, we find that the first order term $\Lambda_{\pm}\epsilon$ generally provides a good approximation of the numerical solution. However, the second order term $\Sigma_{\pm}\epsilon^2$ is required for identifying the physical solutions that satisfy the Sommerfeld condition. The explicit expression for Σ_{\pm} is

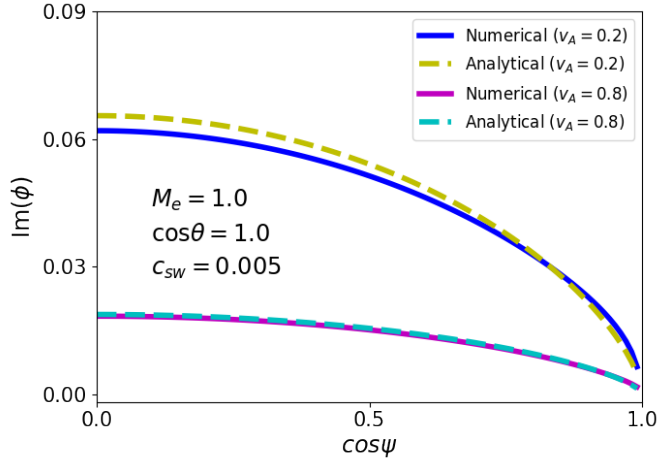


FIG. 4. Dependence of the instability growth rate $\text{Im}(\phi)$ on $\cos\psi$ for two choices of v_A and a fixed value of $\cos\theta = 1$ in the singular case $M_e = 1$. Solid lines represent the numerical solutions while dashed lines represent the analytical solutions obtained by Puiseux series expansion in the main text.

$$\Sigma_{\pm} = \frac{M_e \mu [(1 - M_e^2)(\cos^2 \psi (1 - \eta^2) + M_e^2(1 + 3\eta^2) - 2 - 2M_e^4 \eta^2) \Gamma_w^2 + 2(\cos^2 \psi + M_e^2 - 2)(\mu^2 \pm \lambda)]}{\gamma^2 (1 - M_e^2)^2 \Gamma_w^2 \lambda} \quad (31)$$
